ACS APPLIED MATERIALS & INTERFACES

RESEARCH ARTICLE

www.acsami.org

A Facile Synthesis, In vitro and In vivo MR Studies of D-Glucuronic Acid-Coated Ultrasmall Ln_2O_3 (Ln = Eu, Gd, Dy, Ho, and Er) Nanoparticles as a New Potential MRI Contrast Agent

Krishna Kattel,[†] Ja Young Park,[†] Wenlong Xu,[†] Han Gyeol Kim,[†] Eun Jung Lee,[†] Badrul Alam Bony,[†] Woo Choul Heo,[†] Jae Jun Lee,[‡] Seonguk Jin,[‡] Jong Su Baeck,[‡] Yongmin Chang,[*,‡] Tae Jeong Kim,[§] Ji Eun Bae,[⊥] Kwon Seok Chae,[⊥] and Gang Ho Lee[*,†]

[†]Department of Chemistry, College of Natural Sciences, [§]Department of Applied Chemistry, College of Engineering, and [⊥]Department of Biology Education, Teacher's College, Kyungpook National University, Taegu 702-701, South Korea

[‡]Department of Molecular Medicine and Medical & Biological Engineering, School of Medicine, Kyungpook National University and Hospital, Taegu 702-701, South Korea

Supporting Information

ABSTRACT: A facile one-pot synthesis of D-glucuronic acid-coated ultrasmall Ln_2O_3 (Ln = Eu, Gd, Dy, Ho, and Er) nanoparticles is presented. Their water proton relaxivities were studied to address their possibility as a new potential MRI contrast agent. We focused on the D-glucuronic acid-coated ultrasmall Dy_2O_3 nanoparticle because it showed the highest r_2 relaxivity among studied nanoparticles. Its performance as a T_2 MRI contrast agent was for the first time proved in vivo through its 3 T T_2 MR images of a mouse, showing that it can be further exploited for the rational design of a new T_2 MRI contrast agent at high MR fields.

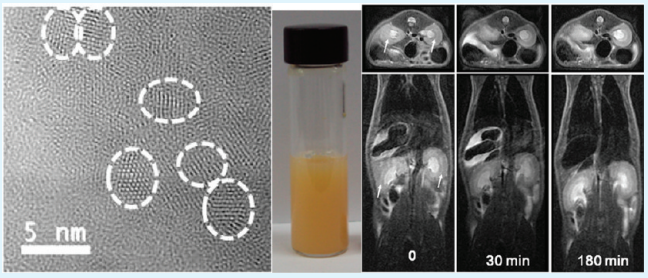

KEYWORDS: Ln_2O_3, ultrasmall nanoparticle, MRI contrast agent, one-pot synthesis

1. INTRODUCTION

Surface coated magnetic nanoparticles have been intensively investigated so far because of their potential applications to a variety of biological and biomedical areas. These include the immobilization[1,2] and the bioseparation[2−4] of biological molecules such as proteins, peptides, enzymes, drug and gene delivery,[2,4,5] magnetic resonance imaging (MRI),[2,4,5] and hyperthermia.[2,4,5] Among these, application of nanoparticles as MRI contrast agents have been actively pursued because they often showed higher water proton relaxivities than molecular chelates. Until now, the iron oxide nanoparticles,[2,5,6] the ferrite nanoparticles,[7] the manganese oxide nanoparticles,[8−10] the gadolinium oxide nanoparticles,[10−20] the gadolinium compound nanoparticles,[21−26] and the dysprosium oxide nanoparticles[26−29] have been investigated. It is interesting to note that some materials such as FeCo nanoparticles[30] as well as the most commonly used iron oxide nanoparticles[31] show very strong both T_1 (or positive) and T_2 (or negative) contrast. This is because they have both high longitudinal (r_1) and transverse (r_2) water proton relaxivities. Among the above nanoparticles, only the dextran-coated iron oxide nanoparticles are now commercially available in the market as a T_2 MRI contrast agent.[6] However, large particle diameters of iron oxide nanoparticles have often limited their clinical applications because they are mostly accumulated in a liver.[32] Therefore, ultrasmall nanoparticles with high water proton relaxivities should be developed to overcome this.

The lanthanide oxide (Ln_2O_3 hereafter) nanoparticles are promising candidates as T_1 and T_2 MRI contrast agents. Two reasons for this include that they are paramagnetic[33−39] and magnetic moments of some Ln(III) are very high. While superparamagnetic nanoparticles such as iron oxide nanoparticles exhibit poor r_2s in the size regime where renal clearance is expected to be efficient,[2,5,7] r_2s of the ultrasmall Ln_2O_3 nanoparticles are significant.[27] The mostly studied Gd_2O_3 nanoparticles have already shown high r_1s at ultrasmall particle diameters.[10−15,17−20] Their capability as a T_1 MRI contrast agent has been also proved in vivo.[15,17] However, they are extremely toxic and thus, should be well-coated with biocompatible ligand. Furthermore, they should be completely cleared out from the body through the bladder in a few hours after injection. The next mostly studied Dy_2O_3 nanoparticles with somewhat large particle diameters have shown high r_2s.[26−28] However, their water proton relaxivities at ultrasmall particle diameters, in vitro cytotoxicity, and in vivo capability as a T_2 MRI contrast agent have not been investigated yet. In this work, we explore, for the

Received: April 9, 2011
Accepted: August 19, 2011
Published: August 19, 2011

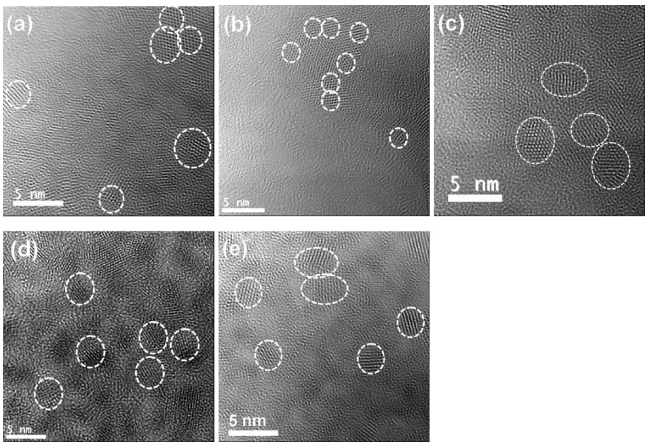

Figure 1. HVEM images of D-glucuronic acid-coated ultrasmall Ln_2O_3 nanoparticles (Ln = (a) Eu, (b) Gd, (c) Dy, (d) Ho, and (e) Er).

first time, their water proton relaxivities, in vitro cytotoxicity, and in vivo capability as a T_2 MRI contrast agent, at ultrasmall particle diameters.

Although a variety of synthetic methods to produce 3*d*-transition metal oxide nanoparticles have been reported so far,[40−44] some of them may not be applied to the lanthanide series. For instance, when lanthanide metal salts react with hydroxide ions in aqueous solution, both $Ln(OH)_3$ nanoparticles and nanorods are produced at ambient temperatures instead of Ln_2O_3 nanoparticles due to high dehydration activation energies from $Ln(OH)_3$ into Ln_2O_3.[45] This is opposite to the 3*d*-transition metal salts which readily form oxides because of low dehydration activation energies of their hydroxides. Therefore, appropriate synthetic methods for Ln_2O_3 nanoparticles should be devised. In this work, we developed a facile synthesis of ultrasmall Ln_2O_3 (Ln = Eu, Gd, Dy, Ho, and Er) nanoparticles. They were then further coated with a biocompatible and water-soluble D-glucuronic acid for both in vitro and in vivo MR experiments without separation. Note that somewhat large lanthanide oxide nanocrystals had been synthesized in organic solvents.[46] However, the synthetic method of the present work is different from the above work. The final products are also different in both morphologies and sizes. The above work provides nanoplates and nanodisks with diameters of 9 to 20 nm, whereas our work provides nearly spherical ultrasmall nanoparticles.

In this work, a facile one-pot synthesis of D-glucuronic acid coated ultrasmall Ln_2O_3 nanoparticles was introduced. Their water proton relaxivities were studied to address their possibility as a new potential MRI contrast agent. Some of colloidal suspensions of these D-glucuronic acid coated nanoparticles in water showed enhanced water proton relaxivities and significant dose-dependent contrast enhancements in their map images. We then focused on D-glucuronic acid-coated ultrasmall Dy_2O_3 nanoparticle due to its high r_2 relaxivity. It was found to be nontoxic in the in vitro cytotoxicity test. Its usefulness as a T_2 MRI contrast agent was for the first time proved in vivo through 3 T T_2 MR images of a mouse.

2. EXPERIMENTAL PROCEDURES

Chemicals. All chemicals such as $GdCl_3.xH_2O$ (99.9%), $Dy(NO_3)_3.5H_2O$ (99.99%), $Er(NO_3)_3.5H_2O$ (99.99%), $Eu(NO_3)_3.5H_2O$ (99.9%), $Ho(NO)_3.5H_2O$ (99.99%), NaOH (>99.9%), 50% H_2O_2 aqueous solution, triethylene glycol (99%), and D-glucuronic acid (99.99%) were purchased from Sigma-Aldrich and used as received. Triply distilled water was used for both washing samples and preparing MRI sample solutions.

Table 1. Average Particle Diameter (d_{avg}), r_1, and r_2 of D-Glucuronic Acid-Coated Ultrasmall Ln_2O_3 Nanoparticles and the *M* of Ln(III) in Ultrasmall Ln_2O_3 Nanoparticles

ultrasmall Ln_2O_3 nanoparticle	d_{avg} (*nm*)	ground state electronic configuration of Ln(III)	*M* at *H* = 5 T (μ_B) 5 K	*M* at *H* = 5 T (μ_B) 300 K	r_1 ($s^{-1}mM^{-1}$)	r_2 ($s^{-1}mM^{-1}$)
Eu_2O_3	2.0	$^7F_0$	0.078	0.046	0.006	3.82
Gd_2O_3	2.4	$^8S_{7/2}$	6.42	0.24	4.25	27.11
Dy_2O_3	2.9	$^6H_{15/2}$	5.19	0.42	0.16	40.28
Ho_2O_3	2.4	$^5I_8$	4.66	0.39	0.13	31.24
Er_2O_3	2.9	$^4I_{15/2}$	4.52	0.34	0.06	14.74

Synthesis of Ultrasmall Ln_2O_3 Nanoparticles. To synthesize ultrasmall Ln_2O_3 nanoparticles, we added 5 mmol of Ln(III) precursor to 30 mL of triethylene glycol in a round-bottom flask. The reaction mixture was magnetically stirred at 50 °C until the precursor was completely dissolved in triethylene glycol. The solution became transparent (solution color, Eu, Gd, and Dy: no color, Ho and Er: pink). Fifteen millimoles of NaOH pellet was then added to the reaction mixture. The reaction temperature was then increased and maintained at 80 °C. The reaction continued until NaOH was completely dissolved over two hours. The solution became cloudy for a while just after the addition of NaOH and then, transparent again (solution color, Eu, Gd, and Dy: yellow, Ho and Er: dark pink). Then, 7.5 *mL* of H_2O_2 aqueous solution was slowly dropped into the reaction mixture through a syringe. The oxygen gas (confirmed from flame experiment) vigorously evolved during the addition of H_2O_2 and the solution became cloudy again with accompanying a color change, due to the formation of ultrasmall Ln_2O_3 nanoparticles (solution color, Eu, Gd, and Dy: white, Ho and Er: pale pink). The reaction mixture was left to react for an additional 2 h. Note that ultrasmall Ln_2O_3 nanoparticles can be also formed without H_2O_2 at high temperatures.[47] However, we found that ultrasmall Ln_2O_3 nanoparticles can be more efficiently formed by adding H_2O_2 even at lower temperature conditions such as those employed here.

Surface Coating of Ultrasmall Ln_2O_3 Nanoparticles with D-Glucuronic Acid. For surface coating of nanoparticles with D-glucuronic acid, 5 *mmol* of D-glucuronic acid was added to the above solution. The surface coating reaction continued for another 6 h. After completion of the reaction, the solution was cooled to room temperature. It was transferred into a 1 *L* beaker containing 500 *mL* of triply distilled water and then, magnetically stirred for an hour. It was stored for a week or so until the D-glucuronic acid coated Ln_2O_3 nanoparticles precipitated. The top transparent solution was decanted and the remaining sample solution was again washed with triply distilled water. This procedure was repeated three times. The first half volume of the sample solution was used to prepare a MRI sample solution in triply distilled water (solution color, Gd and Dy: light yellow, Eu: yellow, and Ho and Er: dark yellow). A typical concentration of the MRI solution was 30 *mM* Ln. The remaining half volume was subjected to a powder form by drying it in air for various characterizations as described below.

Characterization. A high voltage electron microscope (HVEM) (JEOL JEM-ARM 1300S, 1.2 *MeV* acceleration voltage) was used to measure particle diameters of D-glucuronic acid coated ultrasmall Ln_2O_3 nanoparticles. A copper grid (PELCO No.160, TED PELLA, INC.)

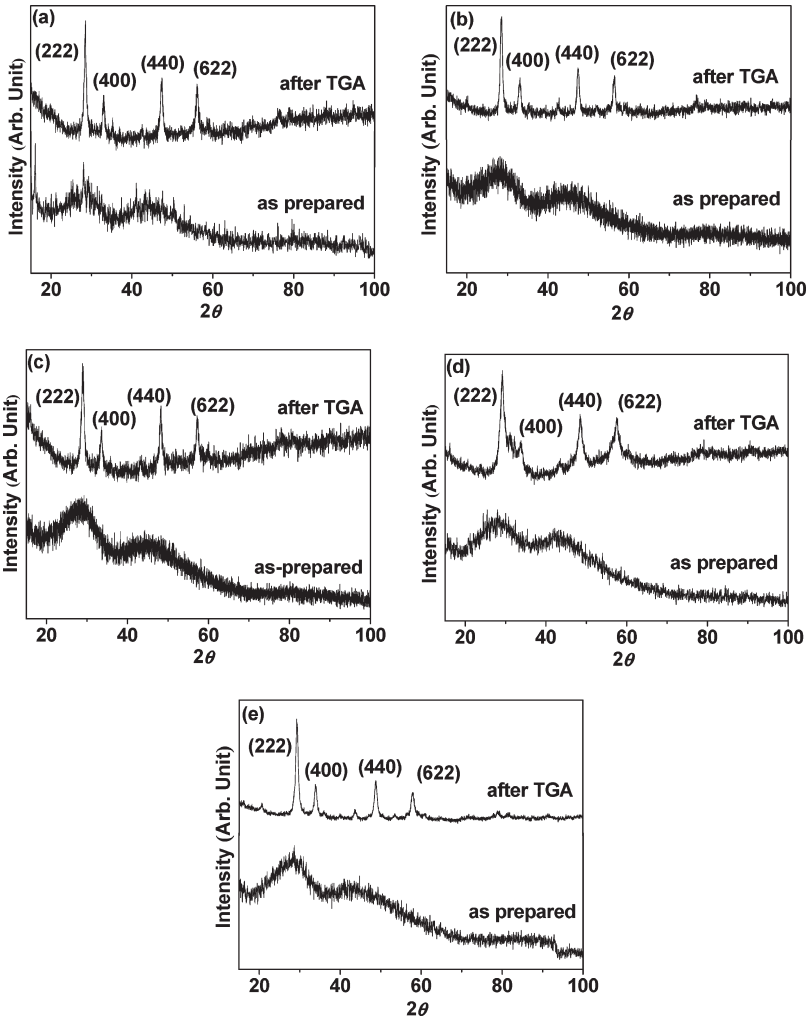

Figure 2. XRD patterns of D-glucuronic acid coated ultrasmall Ln_2O_3 nanoparticles (labeled as "as-prepared") and Ln_2O_3 nanoparticles obtained after TGA analysis up to 700 °C (labeled as "after TGA") (Ln = (a) Eu, (b) Gd, (c) Dy, (d) Ho, and (e) Er).

covered with an amorphous carbon membrane was placed onto a filter paper and then, a sample solution diluted in triply distilled water was dropped over the copper grid by using a micropipet (Eppendorf, 2 - 20 μL). An X-ray diffraction (XRD) spectrometer (Philips, X'PERT PRO MRD) with an unfiltered CuKα (λ = 1.54184 Å) radiation was used to measure crystal structures of D-glucuronic acid coated ultrasmall Ln_2O_3 nanoparticles. The scanning step and the scan range in 2θ were 0.033° and 15 - 100°, respectively. The concentration of Ln in a MRI sample solution was determined by using an inductively coupled plasma atomic emission spectrometer (ICPAES) (Thermo Jarrell Ash Co., IRIS/AP). To determine this, ~ 1 *mL* of the MRI solution was extracted and pretreated with acids to completely dissolve nanoparticles in solution. A Fourier transform-infrared (FT-IR) absorption spectrometer (Mattson Instruments, Inc., Galaxy 7020A) was used to verify the surface coating. To record a FT-IR absorption spectrum (400 - 4000 cm^{-1}), a pellet of a powder sample in KBr was prepared. A thermogravimetric analyzer (TGA) (TA Instruments, SDT-Q 600) was used to estimate the amount of surface coating. A TGA curve of each powder sample was recorded between room temperature and 700 °C while air was flowed. The maximum amount of surface coating with D-glucuronic acid was estimated from the mass drop in the TGA curve. A superconducting quantum interference device (SQUID) magnetometer (Quantum Design, MPMS-7) was used to measure magnetic properties of ultrasmall Ln_2O_3 nanoparticles. Both magnetization (M) versus applied field (H) (*i.e.*, $M - H$) curves ($-5 \leq H \leq 5$ T) at temperatures (T) = 5 and 300 *K* and zero-field-cooled (ZFC) M versus T (*i.e.* M - T) curves ($3 \leq T \leq 330$ *K*) at H = 100 oersted (*Oe*) were recorded. To measure both M - H and M - T curves, each weighed powder sample was loaded into a nonmagnetic gelatin capsule. A very small diamagnetic contribution of the capsule had a negligible contribution to the overall M, which was dominated by the sample. Mass corrected M of each ultrasmall Ln_2O_3 nanoparticle was obtained by using its weight percent estimated from its TGA curve.

r_1 and r_2 Relaxivity and R_1 and R_2 Map Image Measurements. Both R_1 and R_2 map images as well as both T_1 and T_2 relaxation times were measured by using a 1.5 T MRI instrument (GE 1.5 T Signa Advantage, GE medical system) equipped with the knee coil (EXTREM). A series of five aqueous solutions of different concentrations (1, 0.5, 0.25, 0.125, and 0.0625 *mM* Ln) were prepared by diluting each MRI solution with triply distilled water. Then, both map images and relaxation times were measured by using these solutions. The r_1 and r_2 relaxivities were then estimated from the slopes in the plots of $1/T_1$ and $1/T_2$ versus Ln concentration, respectively. The measurement parameters are as follows: the external MR field (H) = 1.5 T, the temperature =22 °C, the number of acquisition (NEX) = 1, the field of view (FOV) = 16 *cm*, the phase FOV = 1, the matrix size = 512 × 512, the slice thickness =5 *mm*, the spacing gap =0, and the pixel bandwidth =61.0547, the repetition time (TR) = 2009 *ms*, and the time to echo (TE) = 9 *ms*.

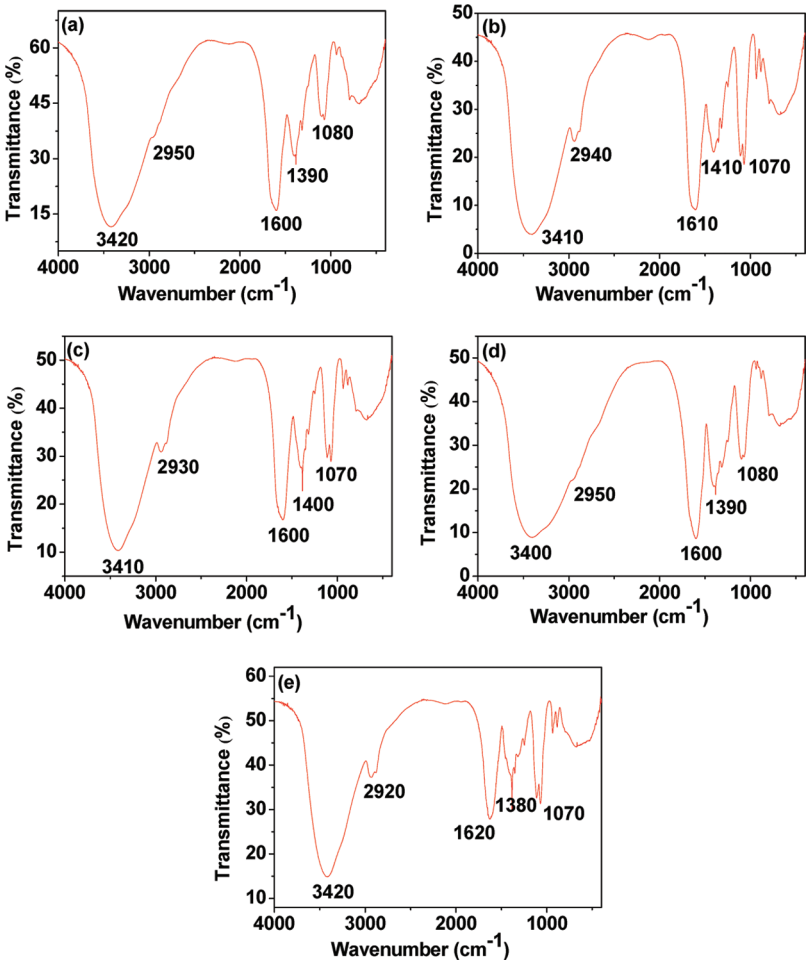

Figure 3. FT-IR absorption spectra of D-glucuronic acid coated ultrasmall Ln_2O_3 nanoparticles (Ln = (a) Eu, (b) Gd, (c) Dy, (d) Ho, and (e) Er).

In vitro Cytotoxicity Test. The cellular toxicity of a Dy_2O_3 MRI solution was measured by using the CellTiter-Glo Luminescent Cell Viability Assay (Promega, WI, USA). In this assay, the intracellular ATP was quantified by using a luminometer (Victor 3, Perkin-Elmer). Both human prostate cancer (DU 145) and normal mouse hepatocyte (NCTC 1469) cell lines were used. Cells were seeded on a 24-well cell culture plate and incubated for 24 h (5×10^4 cell density, 500 μL cells per well, 5% CO_2, 37 °C). Four test solutions (5, 10, 50, and 100 μM Dy) were prepared by diluting the MRI sample solution with a sterile phosphate-buffered saline (PBS) solution. ~ 2 μL of each test solution was treated into the cell culture media. The treated cell culture media were then incubated for 48 h. Each cell viability was measured and normalized with respect to the control cell line with 0.0 *M* Dy concentration. The measurement was repeated three times for each test solution to obtain average cell viabilities.

In vivo T_2 MR Image Measurement. T_2 MR images were taken by using a 3 T MRI scanner (GE 3T, Signa HD). The *in vivo* animal study was performed in accordance with the rules and regulations of the animal research committee of Kyungpook National University. A 6.5 week male ICR mouse with weight of 116 *g* was used. The mouse was anesthetized by 1.5% isoflurane in oxygen. Measurements were made before and after the injection of a MRI solution into a mouse tail vein. The injection dose was 0.05 *mmol* Dy/*kg*. During measurements, the mouse was maintained at 37 °C by using a warm water blanket. After measurements, the mouse was revived from anesthesia and placed in the cage with a free access to both food and water. The measurement parameters are as follows: the *H* = 3 T, the temperature =37 °C, the NEX = 4, the FOV = 6 - 9 *cm*, the phase FOV = 0.7, the matrix size =256 × 256, the slice thickness = 1 - 2 *mm*, the spacing gap =0.5 − 1.0 *mm*, and the pixel bandwidth = 31.25, the TR = 3000 *ms*, the TE = 50 *ms*. Region of interest (ROI) analysis of signal intensities (SI) on T_2 MR images before and after injection was performed by using a circular area of 8.63 mm^2 ROI. The normalized signal intensity was then estimated by dividing SI measured at each time points after injection with SI measured before injection.

3. RESULTS AND DISCUSSION

Particle Diameter and Crystal Structure. HVEM images of D-glucuronic acid coated ultrasmall Ln_2O_3 nanoparticles are shown in Figure 1. The average particle diameters range from 2.0 to 3.0 *nm* as provided in Table 1. By using these HVEM images, we measured particle diameters over 50 to 76 nanoparticles. By using a log-normal distribution function, we fitted the particle diameters (see Supporting Information) and estimated average particle diameters as provided in Table 1. XRD patterns of the as-prepared powder samples are shown in Figure 2. Among the known three phases (i.e., $Ln(OH)_3$, LnOOH, and Ln_2O_3),[45] each obtained XRD pattern is close to that of the Ln_2O_3. The very broad XRD patterns indicate that most of the ultrasmall Ln_2O_3 nanoparticles are not fully crystallized because of their ultrasmall particle diameters, similar to that observed in ultrasmall Gd_2O_3 nanoparticles.[47] After TGA analysis of the powder samples up to 700 °C, however, the sharp peaks (222), (400),

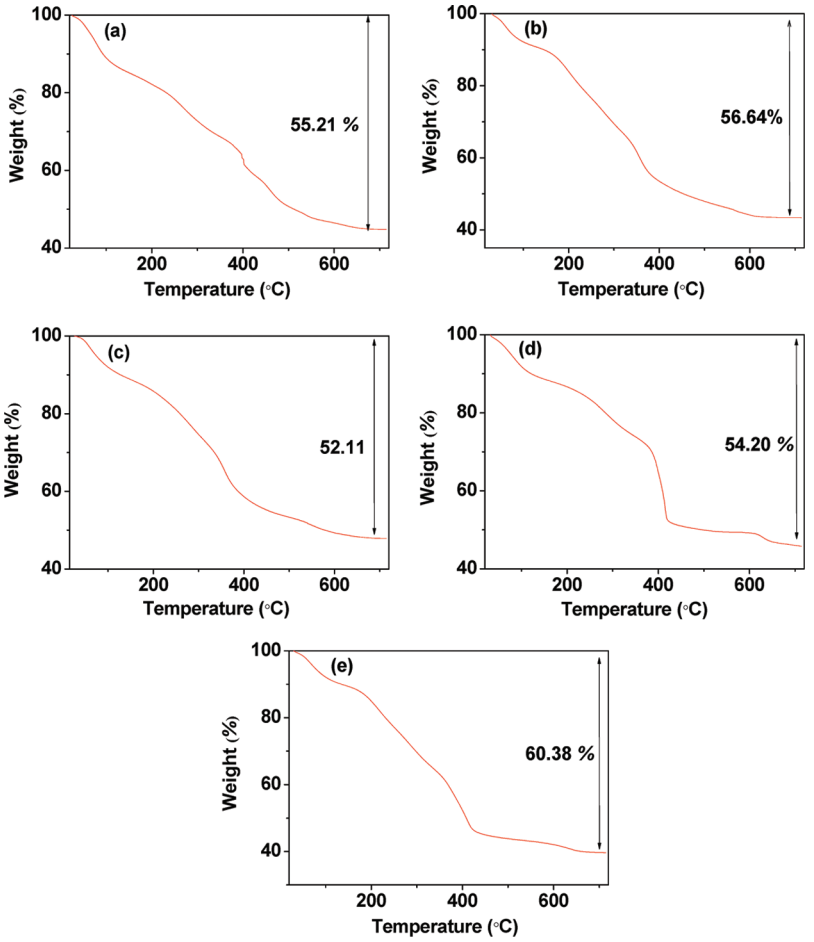

Figure 4. TGA curves of of D-glucuronic acid coated ultrasmall Ln_2O_3 nanoparticles (Ln = (a) Eu, (b) Gd, (c) Dy, (d) Ho, and (e) Er).

Table 2. Grafting Densities and Mass Weight Percents of D-Glucuronic Acids in D-Glucuronic Acid Coated Ultrasmall Ln_2O_3 Nanoparticles

		mass weight percents	
ultrasmall Ln_2O_3 nanoparticle	grafting densities (nm^{-2})	as-prepared	after two months
Eu_2O_3	9.43	55.21	55.46
Gd_2O_3	11.46	56.64	53.45
Dy_2O_3	12.74	52.11	54.87
Ho_2O_3	12.35	54.20	56.91
Er_2O_3	19.74	60.38	59.89

(440), and (622), corresponding to a highly crystallized form of Ln_2O_3 with a cubic structure, were observed as shown in Figure 2. The particle diameters after TGA analysis also increased, ranging from 5 to 15 nm (see HVEM images in the Supporting Information). The estimated cell constants of these samples are consistent with the values given by JCPDS-International Center for Diffraction Data, PCPDFWIN, Version 1.30 (Table S1 in Supporting Information).[48]

Surface Coating. FT-IR absorption spectra are shown in Figure 3. The characteristic stretching frequencies at 2920−2950, 1600−1620, and 1070−1080 cm^{-1}, corresponding to the C−H, the C═O, and the C−O stretches, respectively, confirm that ultrasmall Ln_2O_3 nanoparticles are coated with D-glucuronic acid. The red shift in the C═O stretch by ∼100 cm^{-1} from ∼1710 cm^{-1} of a free D-glucuronic acid confirms that the carboxylic acid group chemically binds to surface Ln(III). This red shift had been already observed in various metal oxide nanoparticles coated by various ligands with carboxylic acid groups.[47,49,50] The peak at 1380−1410 cm^{-1} results from the stretching absorption of CO_3^{2-}, which was formed from the reaction between absorbed water and CO_2 from air.[51,52] The TGA curves in Figure 4 show that the ultrasmall nanoparticles are sufficiently coated with D-glucuronic acid, which is prerequisite for biomedical applications. The maximum surface coatings by D-glucuronic acid were estimated to be 55.21, 56.64, 52.11, 54.20, and 60.38% in weight percent for ultrasmall Ln_2O_3 nanoparticles (Ln = Eu, Gd, Dy, Ho, and Er, respectively). From these, net masses of ultrasmall Ln_2O_3 nanoparticles in D-glucuronic acid coated ultrasmall Ln_2O_3 nanoparticles were estimated to be 44.79, 43.36, 47.89, 45.80, and 39.62% for Ln = Eu, Gd, Dy, Ho, and Er, respectively, and used for estimating net (or mass corrected) *Ms* of the ultrasmall Ln_2O_3 nanoparticles in D-glucuronic acid-coated ultrasmall Ln_2O_3 nanoparticles.

To estimate the number of D-glucuronic acids on unit area of a nanoparticle surface, we calculated grafting densities[53] by using a molecular mass of D-glucuronic acid of 194.14 g/mol, average particle diameters estimated from HVEM images (Table 1), and bulk densities of 7.42 (Eu_2O_3), 7.407 (Gd_2O_3), 7.42 (Dy_2O_3),

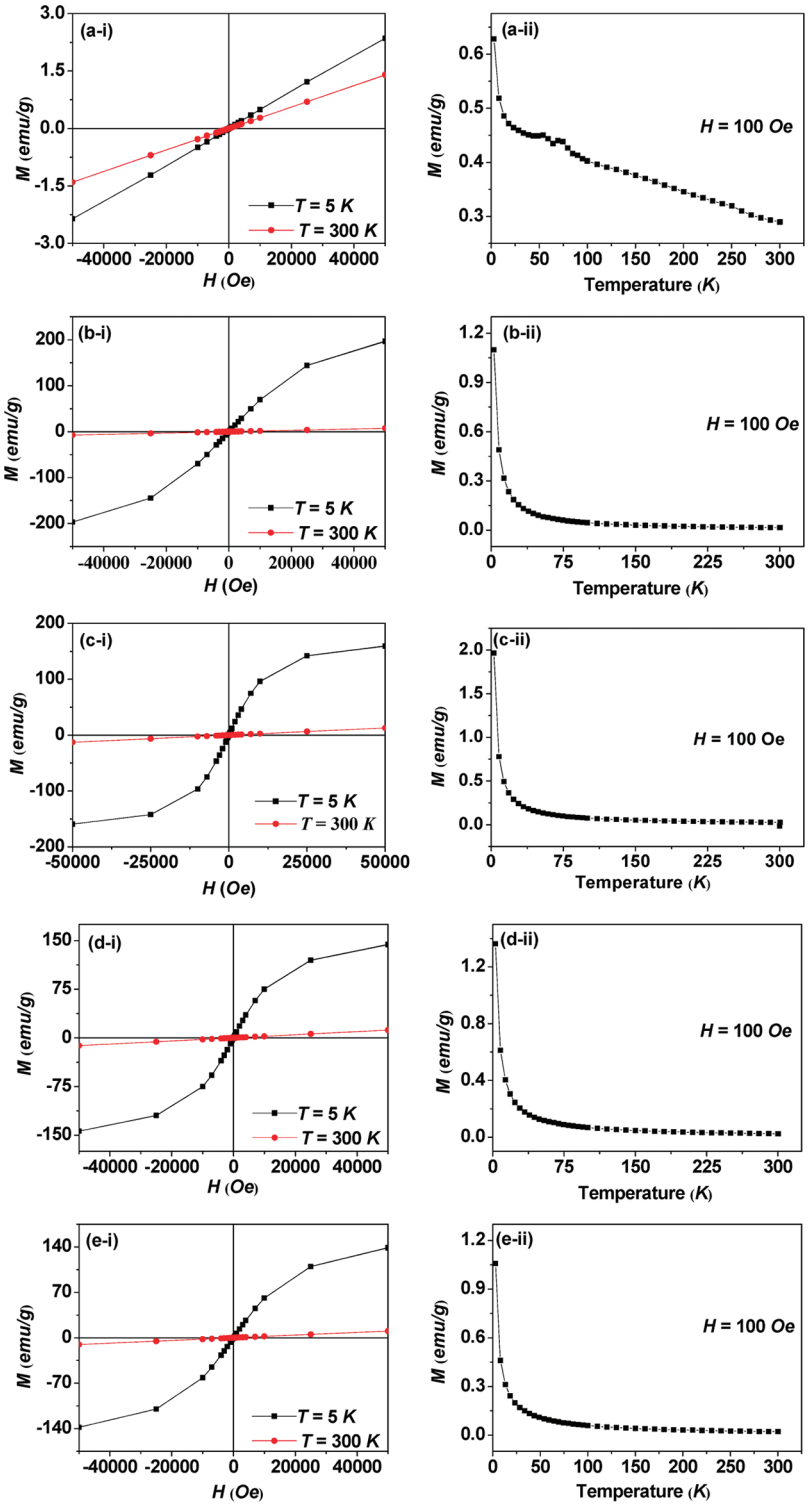

Figure 5. Both (i) mass corrected $M-H$, and (ii) $M-T$ curves of D-glucuronic acid-coated ultrasmall Ln_2O_3 nanoparticles (Ln = (a) Eu, (b) Gd, (c) Dy, (d) Ho, and (e) Er).

8.41 (Ho_2O_3), and 8.64 g/mL (Er_2O_3).[54] As provided in Table 2, grafting densities are all large, implying that nanoparticles are sufficiently coated with D-glucuronic acids. Furthermore, for surface coating stabilities to be measured, the nanoparticle solutions sit 2 months until nanoparticles precipitate. The top clear solutions were decanted. If surface coating was unstable, ligands will be liberated into solution phase. The remaining precipitated nanoparticles were collected and dried in air and then, subject to TGA analysis (see the Supporting Information for TGA curves). The mass percentages of ligands were compared to the previous values of as-prepared samples. As given in Table 2, the differences are negligible within an experimental error limit, implying that ligand coatings are stable.

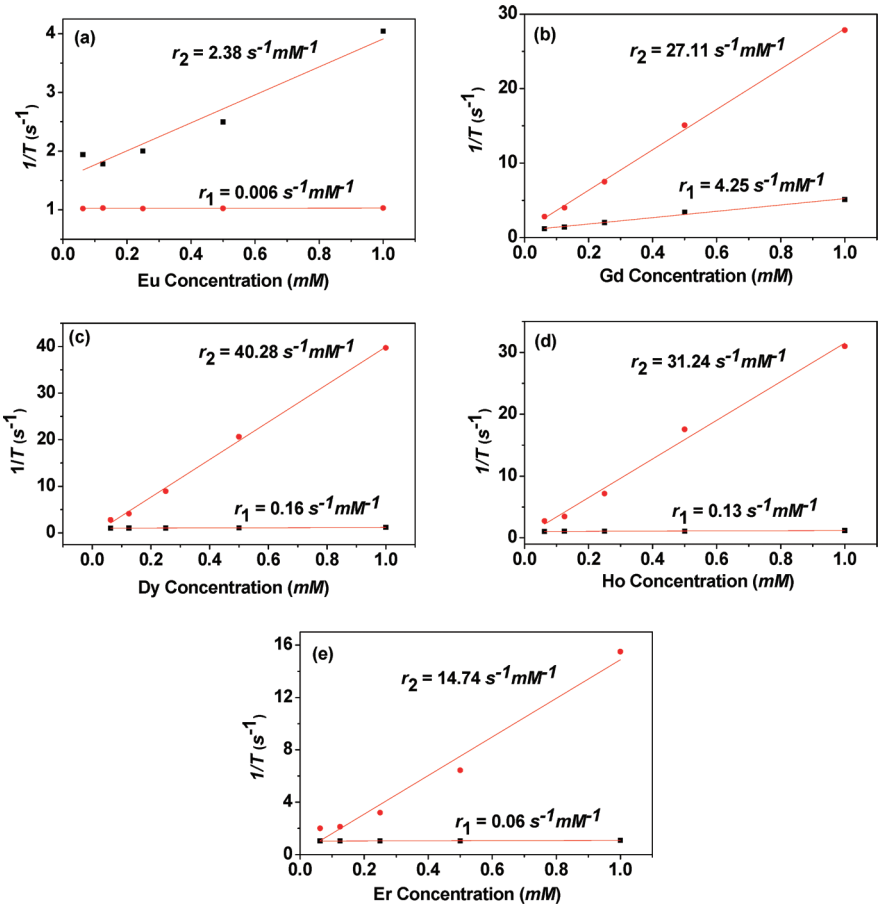

Figure 6. Plots of $1/T_1$ and $1/T_2$ inverse relaxation times of sample solutions of D-glucuronic acid coated ultrasmall Ln_2O_3 nanoparticles (Ln = (a) Eu, (b) Gd, (c) Dy, (d) Ho, and (e) Er). The slopes correspond to r_1 and r_2 relaxivities, respectively.

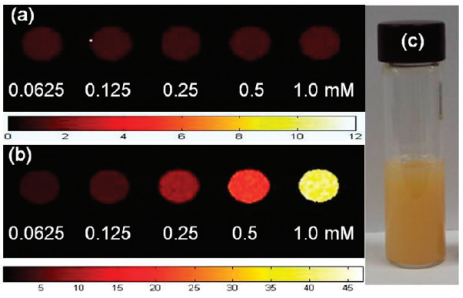

Figure 7. Both (a) R_1 and (b) R_2 map images as a function of Dy concentration, and (c) a Dy_2O_3 MRI sample solution.

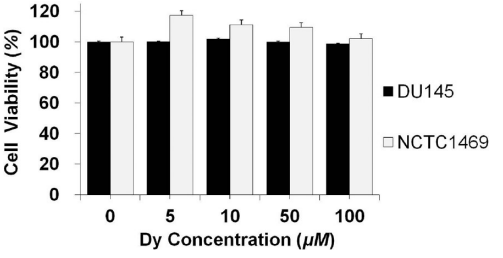

Figure 8. In vitro cytotoxicity tests of a Dy_2O_3 MRI sample solution by using DU 145 and NCTC 1469 cell lines.

Magnetic Properties. Both mass corrected ZFC $M-T$ curves at H = 100 Oe and $M-H$ curves at T = 5 and 300 K are shown in Figure 5. The mass corrected Ms are due to ultrasmall Ln_2O_3 nanoparticles. The $M-H$ curves at both T = 5 and 300 K show that both coercivity and remanance are zero (i.e., no hysteresis). This lack of hysteresis as well as no magnetic transition down to T = 3 K in the ZFC $M-T$ curves shows that all samples are paramagnetic down to T = 3 K. These are consistent with experiments.[33−39] From the $M-H$ curves, the Ms at H = 5 T were estimated and then, multiplied by $m(Ln_2O_3)/2m(Ln)$ to get net Ms of Ln(III) in ultrasmall Ln_2O_3 nanoparticles (Table 1). These values at T = 5 K except for that of ultrasmall Eu_2O_3 nanoparticles are somewhat lower than those of expected values[55] because of some errors in sample masses as well as because the M − H curves are not fully saturated at H = 5 T. Here, ultrasmall Eu_2O_3 nanoparticle shows a negligible M because the total electron angular momentum (J) of Eu(III) = 0. The magnitude of M at room temperature is very important for determining both r_1 and r_2.[28,56] Furthermore, the r_1 is very high when the M solely arises from S-state electrons of Ln(III) as discussed below.[56]

r_1 and r_2 Relaxivities and R_1 and R_2 Map Images. Both inverse longitudinal $(1/T_1)$ and transverse $(1/T_2)$ relaxation times are plotted as a function of Ln concentration as shown in Figure 6 and then, both r_1 and r_2 are obtained from the slopes, respectively, as provided in Table 1. It is known that only the electron spin magnetic moment can efficiently induce the

longitudinal water proton relaxation because a slow electron spin motion is closely in match with a slow water proton relaxation.[56] However, a fast electron orbital motion is quite far from the water proton relaxation. Therefore, r_1 will be high if **J** of Ln(III) consists only of the electron spin angular momentum (**S**) and is also high. But it will be small if **J** has a contribution from an electron orbital angular momentum (**L**). This explains why only the D-glucuronic acid coated ultrasmall Gd_2O_3 nanoparticle has a high r_1, whereas others have negligible r_1s (see Table 1). As a consequence, only the D-glucuronic acid coated ultrasmall Gd_2O_3 nanoparticle shows a clear dose-dependent contrast enhancement in its R_1 map image (see Figure 7a for D-glucuronic acid coated ultrasmall Dy_2O_3 nanoparticle and Supporting Information for others). On the other hand, r_2 is roughly proportional to the M^2 of nanoparticle at room temperature.[28] Therefore, as expected, the D-glucuronic acid coated ultrasmall Dy_2O_3 nanoparticle shows the highest r_2 (see Table 1) and as a result, the most clear dose-dependent contrast enhancement in its R_2 map image among the studied nanoparticles (see Figure 7b for the D-glucuronic acid coated ultrasmall Dy_2O_3 nanoparticle and the Supporting Information for others).

Based on the above estimated r_1 and r_2, D-glucuronic acid-coated ultrasmall Gd_2O_3 and Dy_2O_3 nanoparticles are the best candidates for T_1 and T_2 MRI contrast agents among the studied nanoparticles, respectively. As mentioned before, Gd_2O_3 nanoparticles have been intensively studied in vitro and in vivo,[10−15,17−20] whereas only a few studies on Dy_2O_3 nanoparticle exist.[26−29] Therefore, we will concentrate on the role of the D-glucuronic acid coated ultrasmall Dy_2O_3 nanoparticle as T_2

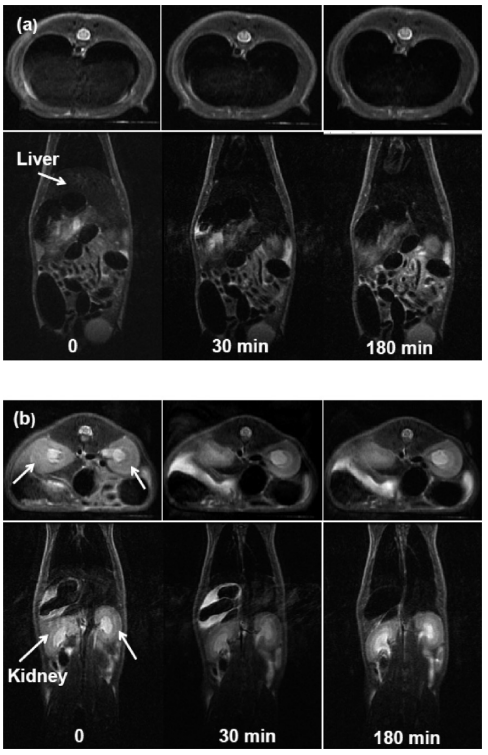

Figure 9. Series of axial (top) and coronal (bottom) 3 T T_2 MR images of (a) liver and (b) kidneys (indicated with arrows) of a mouse with time after the injection of a Dy_2O_3 MRI sample solution into a mouse tail vein.

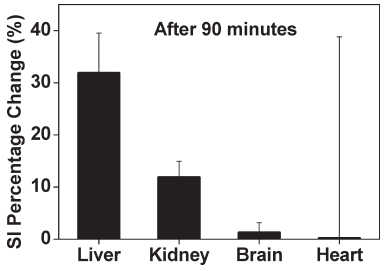

Figure 11. Percentage change of the normalized SI in liver, kidney, brain, and heart at 90 min after injection of the Dy_2O_3 MRI sample solution into a mouse tail vein. This roughly shows biodistribution of nanoparticles at this time.

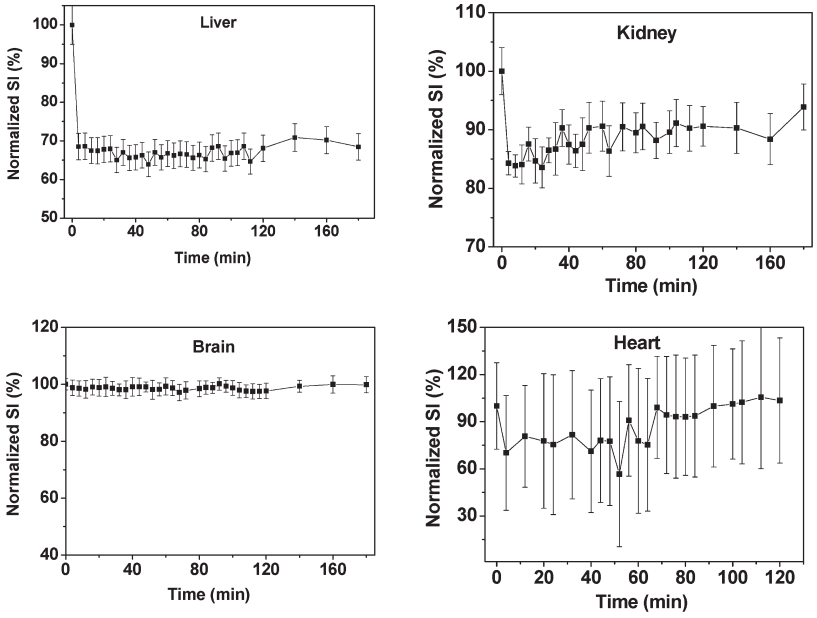

Figure 10. Normalized SI as a function of time in liver, kidney, brain, and heart after injection of the Dy_2O_3 MRI sample solution into a mouse tail vein.

MRI contrast agents. Here, water proton relaxivities, in vitro cytotoxicity, and in vivo MR imaging properties associated with the D-glucuronic acid-coated ultrasmall Dy_2O_3 nanoparticles are exploited for the first time. A well-dispersed Dy_2O_3 MRI sample solution is shown in Figure 7c.

To evaluate the coating effectiveness, we measured both r_1 and r_2 relaxivities on ultrasmall Dy_2O_3 nanoparticles without D-glucuronic acid coating. They are estimated to be 0.05 and 54.26 s^{-1} mM^{-1}, respectively (see the Supporting Information). The measured r_2 is somewhat larger than that of D-glucuronic acid-coated ultrasmall Dy_2O_3 nanoparticles. This is likely due to the different coating states between them.[56,57] That is, the water can more closely approach less coated or uncoated nanoparticles than coated nanoparticles. Thus, the water proton can feel stronger local magnetic fields from the former than the latter. As a result, the former can more efficiently induce water proton relaxations than the latter, making r_2 of the former larger than that of the latter. Here, note that solvent coating can not be totally avoided because nanoparticles were synthesized in triethylene glycol. Thus, some solvent coating is expected for ultrasmall Dy_2O_3 nanoparticles without D-glucuronic acid coating.

In vitro Cytotoxicity. Prior to the in vivo animal experiments, a cytotoxicity test of a Dy_2O_3 MRI sample solution was performed. As shown in Figure 8, the nanoparticles are nontoxic for the tested concentration range up to 100 μM Dy and thus, safe for in vivo experiments. We also measured the cell viability on ultrasmall Dy_2O_3 nanoparticles without D-glucuronic acid coating. It is found that these nanoparticles are nearly nontoxic for the tested concentration range up to 100 μM Dy (see the Supporting Information), similar to that observed in D-glucuronic acid coated ultrasmall Dy_2O_3 nanoparticles. This is likely because Dy(III) is not much toxic within the tested concentration range.[58,59] In addition to this, some solvent coating as mentioned above will further reduce any toxicity of nanoparticles.

In vivo T_2 MR Images of a Mouse. To find out whether or not the D-glucuronic acid coated ultrasmall Dy_2O_3 nanoparticle can be a potential T_2 MRI contrast agent, an in vivo animal experiment was performed at 3 T MR field. The MRI sample solution was injected into a mouse tail vein and a series of 3 T in vivo T_2 MR images were taken with time. The results are provided in Figure 9. A strong negative (i.e., darker) contrast enhancement in liver can be clearly seen in T_2 MR images after 30 min of injection of the Dy_2O_3 MRI sample solution (Figure 9a). Although weaker than liver, the kidneys also show a negative contrast enhancement after 30 min (Figure 9b). The strong signal intensity (SI) change in the liver suggests that the nanoparticles were taken up by the reticuloendothelial system of liver. Furthermore, the negative contrast enhancement in the kidneys demonstrates that the nanoparticles were in part cleared out by the kidneys, which is important for a clinical application. Figure 10 shows the normalized SI as a function of time in liver, kidney, brain, and heart after injection of the Dy_2O_3 MRI sample solution. Liver shows the negative contrast enhancement up to 180 min after injection while the kidneys do not keep the negative contrast enhancement at 180 min. These results were expected in that the clearance of nanoparticles by the reticuloendothelial system of liver is known to take up to a month but the clearance by glomerular filtration through kidneys is much faster.[60] Compared to in vivo work by using silanized Dy_2O_3:Tb^{3+} nanocrystals,[29] our T_2 MR images show definite negative contrast enhancements because the r_2 of D-glucuronic acid coated ultrasmall Dy_2O_3 nanoparticles of this work is much higher than that of silanized Dy_2O_3:Tb^{3+} nanocrystals.

Biodistribution of injected nanoparticles was investigated by using the change of the normalized SI in various organs at 90 min after injection (Figure 11). Note that the change in the normalized SI is proportional to the amount of accumulated nanoparticles. As can be seen in Figure 11, the nanoparticles are highly accumulated in the liver but less accumulated in the kidneys. However, the nanoparticles were negligibly accumulated in brain and heart at this time.

Considering that r_2 is roughly proportional to the M^2 of nanoparticle as mentioned before, this negative contrast enhancement will become even stronger at higher MR fields because the M increases as the MR field strength increases. Therefore, T_2 MR images should be more exploited at high MR fields.

4. CONCLUSION

We developed a new and facile one-pot synthesis of D-glucuronic acid coated ultrasmall Ln_2O_3 (Ln = Eu, Gd, Dy, Ho, and Er) nanoparticles. We investigated their application as new MRI contrast agents by measuring their water proton relaxivities. The D-glucuronic acid coated ultrasmall Gd_2O_3 nanoparticle showed a high r_1 (= 4.25 s^{-1} mM^{-1}), whereas others showed negligible r_1s (<0.2 s^{-1} mM^{-1}). Therefore, only the D-glucuronic acid-coated ultrasmall Gd_2O_3 nanoparticle is a potential candidate for a T_1 MRI contrast agent. The D-glucuronic acid-coated ultrasmall Dy_2O_3 nanoparticle showed the highest r_2 (= 40.28 s^{-1} mM^{-1}) among the studied nanoparticles. It was found to be nontoxic up to 100 μM Dy in cytotoxicity test. It showed a clear but weak negative contrast enhancement in its T_2 MR images of a mouse at 3 T MR field, as expected from the moderate r_2. This suggests that it can be further exploited for the rational design of a new T_2 MRI contrast agent at high MR fields because r_2 rapidly increases with increasing MR field strengths. Also, biodistribution of nanoparticles after sacrificing a rat should be performed. Because r_2 is somewhat affected by both coating agents and particle diameters, different coating agents as well as different synthesis to get different particle diameters may be also tried. If developed, it may be used either target-specifically or non-target-specifically because of its ultrasmall size like molecular MRI contrast agents.

■ ASSOCIATED CONTENT

Supporting Information. Additional information including particle diameter distributions and log-normal function fits, TGA curves to check coating stability, r_1 and r_2 relaxivities and cell viabilities of ultrasmall Dy_2O_3 nanoparticles without D-glucuronic acid coating, R_1 and R_2 map images, MRI sample solution pictures of D-glucuronic acid-coated ultrasmall Ln_2O_3 (Ln = Eu, Gd, Ho, and Er) nanoparticles, HVEM images and cell constants of TGA-analyzed Ln_2O_3 (Ln = Eu, Gd, Dy, Ho, and Er) nanoparticles. This material is available free of charge via the Internet at http://pubs.acs.org.

■ AUTHOR INFORMATION

Corresponding Author

*Tel: -82-53-950-5340 (G.H.L.); -82-53-420-5471 (Y.C.). Fax: -82-53-950-6330 (G.H.L.). E-mail: ghlee@mail.knu.ac.kr (G.H.L.); ychang@knu.ac.kr (Y.C.).

■ ACKNOWLEDGMENT

This work was supported by Grant RTI04-01-01 from the Regional Technology Innovation Program of the Ministry of Commerce, Industry, and Energy funded by the Korean Government, the Basic Science Research Program through the National Research Foundation (NRF) funded by the Ministry of Education, Science and Technology (2010-0002436), and the Ministry for Health, Welfare & Family Affairs through the Korea Healthcare technology R&D Project (Grant A090193). We thank the Korea Basic Science Institute for allowing us to use their HVEM.

■ REFERENCES

(1) Kouassi, G. K.; Irudayaraj, J. *J. Nanobiotechnol.* **2006**, *4*, 8.
(2) Pankhurst, Q. A.; Connolly, J.; Jones, S. K.; Dobson, J. *J. Phys. D: Appl. Phys.* **2003**, *36*, R167–R181.
(3) Doyle, P. S.; Bibette, J.; Bancaud, A.; Viovy, J.-L. *Science* **2002**, *295*, 2237.
(4) Salata, O. V. *J. Nanobiotechnol.* **2004**, *2*, 3.
(5) Pankhurst, Q. A.; Thanh, N. K. T.; Jones, S. K.; Dobson, J. *J. Phys. D: Appl. Phys.* **2009**, *42*, 224001–224015.
(6) *Resovist*; Schering AG: Berlin, Germany.
(7) Lee, J.-H.; Huh, Y.-M.; Jun, Y.-W.; Seo, J.-W.; Jang, J.-T.; Song, H.-T.; Kim, S.; Cho, E.-J.; Yoon, H.-G.; Suh, J.-S.; Cheon, J. *Nat. Med.* **2007**, *13*, 95–99.
(8) Na, H. B.; Lee, J. H.; An, K.; Park, Y. I.; Park, M.; Lee, I. S.; Nam, D.-H.; Kim, S. T.; Kim, S.-H.; Kim, S.-W.; Lim, K.-H.; Kim, K.-S.; Kim, S.-O.; Hyeon, T. *Angew. Chem., Int. Ed.* **2007**, *46*, 5397–5401.
(9) Baek, M. J.; Park, J. Y.; Xu, W.; Kattel, K.; Kim, H. G.; Lee, E. J.; Patel, A. K.; Lee, J. J.; Chang, Y.; Kim, T. J.; Bae, J. E.; Chae, K. S.; Lee, G. H. *ACS Appl. Mater. Interfaces* **2010**, *2*, 2949–2955.
(10) Park, J. Y.; Choi, E. S.; Baek, M. J.; Lee, G. H.; Woo, S.; Chang, Y. *Eur. J. Inorg. Chem.* **2009**, 2477–2481.
(11) Choi, E. S.; Park, J. Y.; Baek, M. J.; Xu, W.; Kattel, K.; Kim, J. H.; Lee, J. J.; Chang, Y.; Kim, T. J.; Bae, J. E.; Chae, K. S.; Suh, K. J.; Lee, G. H. *Eur. J. Inorg. Chem.* **2010**, 4555–4560.
(12) Engström, M.; Klasson, A.; Pedersen, H.; Vahlberg, C.; Käll, P.-O.; Uvdal, K. *Magn. Reson. Mater. Phys.* **2006**, *19*, 180–186.
(13) Fortin, M.-A.; Petoral, R. M.; Söderlind, F.; Klasson, A.; Engström, M.; Veres, T.; Käll, P. −O.; Uvdal, K. *Nanotechnology* **2007**, *18*, 395501 (9 page).
(14) Petoral, R. M.; Söderlind, F.; Klasson, A.; Suska, A.; Fortin, M. A.; Abrikossova, N.; Selegård, L.; Käll, P.-O.; Engström, M.; Uvdal, K. *J. Phys. Chem. C* **2009**, *113*, 6913–6920.
(15) Bridot, J.-L.; Faure, A.-C.; Laurent, S.; Rivière, C.; Billotey, C.; Hiba, B.; Janier, M.; Josserand, V.; Coll, J.-L.; Elst, L. V.; Muller, R.; Roux, S.; Perriat, P.; Tillement, O. *J. Am. Chem. Soc.* **2007**, *129*, 5076–5084.
(16) Miyawaki, J.; Yudasaka, M.; Imai, H.; Yorimitsu, H.; Isobe, H.; Nakamura, E.; Iijima, S. *J. Phys. Chem. B* **2006**, *110*, 5179–5181.
(17) Park, J. Y.; Baek, M. J.; Choi, E. S.; Woo, S.; Kim, J. H.; Kim, T. J.; Jung, J. C.; Chae, K. S.; Chang, Y.; Lee, G. H. *ACS Nano* **2009**, *3*, 3663–3669.
(18) Li, I.-F.; Su, C.-H.; Sheu, H.-S.; Chiu, H.-C.; Lo, Y.-W.; Lin, W.-T.; Chen, J.-H.; Yeh, C.-S. *Adv. Funct. Mater.* **2008**, *18*, 766–776.
(19) Hu, K.-W.; Jhang, F.-Y.; Su, C.-H.; Yeh, C.-S. *J. Mater. Chem.* **2009**, *19*, 2147–2153.
(20) Ahrén, M.; Selegård, L.; Klasson, A.; Söderlind, F.; Abrikossova, N.; Skoglund, C.; Bengtsson, T.; Engström, M.; Käll, P.-O.; Uvdal, K. *Langmuir* **2010**, *26*, 5753–5762.
(21) Rieter, W. J.; Taylor, K. M. L.; An, H.; Lin, W.; Lin, W. *J. Am. Chem. Soc.* **2006**, *128*, 9024–9025.
(22) Li, I.-F.; Yeh, C.-S. *J. Mater. Chem.* **2010**, *20*, 2079–2081.
(23) Hifumi, H.; Yamaoka, S.; Tanimoto, A.; Citterio, D.; Suzuki, K. *J. Am. Chem. Soc.* **2006**, *128*, 15090–15091.
(24) Evanics, F.; Diamente, P. R.; van Veggel, F. C. J. M.; Stanisz, G. J.; Prosser, R. S. *Chem. Mater.* **2006**, *18*, 2499–2505.
(25) Yoon, Y.; Lee, B.-I.; Lee, K. S.; Heo, H.; Lee, J. H.; Byeon, S.-H.; Lee, I. S. *Chem. Commun.* **2010**, *46*, 3654–3656.
(26) Gossuin, Y.; Hocq, A.; Vuong, Q. L.; Disch, S.; Hermann, R. P.; Gillis, P. *Nanotechnology* **2008**, *19*, 475102 (8 page).
(27) Norek, M.; Kampert, E.; Zeitler, U.; Peters, J. A. *J. Am. Chem. Soc.* **2008**, *130*, 5335–5340.
(28) Norek, M.; Pereira, G. A.; Geraldes, C. F. G. C.; Denkova, A.; Zhou, W.; Peters, J. A. *J. Phys. Chem. C* **2007**, *111*, 10240–10246.
(29) Das, G. K.; Zhang, Y.; D'Silva, L.; Padmanabhan, P.; Heng, B. C.; Loo, J. S. C.; Selvan, S. T.; Bhakoo, K. K.; Tan, T. T. Y. *Chem. Mater.* **2011**, *23*, 2439–2446.
(30) Seo, W. S.; Lee, J. H.; Sun, X.; Suzuki, Y.; Mann, D.; Liu, Z.; Terashima, M.; Yang, P. C.; McConnell, M. V.; Nishimura, D. G.; Dai, H. *Nat. Mater.* **2006**, *5*, 971–976.
(31) Cunningham, C. H.; Arai, T.; Yang, P. C.; McConnell, M. V.; Pauly, J. M.; Conolly, S. M. *Magn. Reson. Med.* **2005**, *53*, 999–1005.
(32) Weissleder, R.; Elizondo, G.; Wittenberg, J.; Rabito, C. A.; Bengele, H. H.; Josephson, L. *Radiology* **1990**, *175*, 489–493.
(33) Arajs, S.; Colvin, R. V. *J. Appl. Phys.* **1964**, *35*, 1181–1183.
(34) Moon, R. M.; Koehler, W. C. *Phys. Rev. B* **1975**, *11*, 1609–1622.
(35) Arajs, S.; Colvin, R. V. *J. Appl. Phys.* **1962**, *33*, 2517–2519.
(36) Koehler, W. C.; Wollan, E. O.; Wilkinson, M. K. *Phys. Rev.* **1958**, *110*, 37–40.
(37) Lal, H. B.; Pratap, V.; Kumar, A. *Pramana* **1978**, *10*, 409–412.
(38) Moon, R. M.; Koehler, W. C.; Child, H. R.; Raubenheimer, L. J. *Phys. Rev.* **1968**, *176*, 722–731.
(39) Blanusa, J.; Antic, B.; Kremenovic, A.; Nikolic, A. S.; Mazzerolles, L.; Mentus, S.; Spasojevic, V. *Solid State Commun.* **2007**, *144*, 310–314.
(40) Cornell, R. M.; Schwertmann, U. *The Iron Oxides*; VCH: Weinheim, Germany, 1996; pp 493.
(41) Jana, N. R.; Chen, Y.; Peng, X. *Chem. Mater.* **2004**, *16*, 3931–3935.
(42) Hyeon, T.; Lee, S. S.; Park, J.; Chung, Y.; Na, H. B. *J. Am. Chem. Soc.* **2001**, *123*, 12798–12801.
(43) Sun, S.; Zeng, H. *J. Am. Chem. Soc.* **2002**, *124*, 8204–8205.
(44) Li, Z.; Sun, Q.; Gao, M. *Angew. Chem., Int. Ed.* **2005**, *44*, 123–126.
(45) Chang, C.; Mao, D. *Int. J. Chem. Kinet.* **2007**, *39*, 75–81.
(46) Si, R.; Zhang, Y. −W.; Zhou, H. −P.; Sun, L. −D.; Yan, C. −H. *Chem. Mater.* **2007**, *19*, 18–27.
(47) Söderlind, F.; Pedersen, H.; Petoral, R. M.; Käll, P. O.; Uvdal, K. *J. Colloid Interface Sci.* **2005**, *288*, 140–148.
(48) JCPDS-International Centre for Diffraction Data, card 43−1008, 43−1014, 43−1006, 44−1268, 43−1007 for Eu_2O_3, Gd_2O_3, Dy_2O_3, Ho_2O_3, and Er_2O_3, respectively.
(49) Mendive, C. B.; Bredow, T.; Blesa, M. A.; Bahnemann, D. W. *Phys. Chem. Chem. Phys.* **2006**, *8*, 3232–3247.
(50) Roddick-Lanzilotta, A. D.; McQuillan, A. J. *J. Colloid Interface Sci.* **1999**, *217*, 194–202.
(51) Li, Y.; Ooi, C. P.; Cheang, P. H. N. *Int. J. Appl. Ceram. Technol.* **2009**, *6*, 501–512.
(52) Legodi, M. A.; de Waal, D.; Potgieter, J. H.; Potgieter, S. S. *Miner. Eng.* **2001**, *14*, 1107–1111.
(53) Corbierre, M. K.; Cameron, N. S.; Lennox, R. B. *Langmuir* **2004**, *20*, 2867–2873.
(54) Bulk densities are obtained from Aldrich, 2009−2010.
(55) O'Handley, R. C. *Modern Magnetic Materials*; Wiley-Interscience: New York, 2000; p 492.
(56) Caravan, P.; Ellison, J. J.; McMurry, T. J.; Lauffer, R. B. *Chem. Rev.* **1999**, *99*, 2293–2352.
(57) Park, J.-A.; Lee, J.-J.; Kim, I.-S.; Park, B.-H.; Lee, G. H.; Kim, T. J.; Ri, H.-C.; Kim, H.-J.; Chang, Y. *Colloids Surf., A* **2008**, *313−314*, 288–291.
(58) Heng, B. C.; Das, G. K.; Zhao, X.; Ma, L. L.; Tan, T. T.; Ng, K. W.; Loo, J. S. *Biointerphases* **2010**, *5*, FA88–97.
(59) Emsley, J. *Nature's Building Blocks*; Oxford University Press: Oxford, U.K., 2001; p 130.
(60) Lawaczek, R.; Menzel, M.; Pietsch, H. *Appl. Organomet. Chem.* **2004**, *18*, 506–513.